Health Prognostics of Lithium-ion Batteries and Battery-Integrated Structure

4 authors, including:

Purim Ladpli
Stanford University
20 PUBLICATIONS   **174** CITATIONS

SEE PROFILE

Fotis Kopsaftopoulos
Rensselaer Polytechnic Institute
85 PUBLICATIONS   **818** CITATIONS

SEE PROFILE

fu-kuo Chang
Stanford University
255 PUBLICATIONS   **10,336** CITATIONS

SEE PROFILE

Some of the authors of this publication are also working on these related projects:

Formal Verification of Stochastic State Awareness for Dynamic Data-Driven In- telligent Aerospace Systems View project

Rotor Fault Detection and Identification on VTOL Vehicles Based on Statistical Learning and Time Series Methods View project

Health Prognostics of Lithium-ion Batteries and Battery-Integrated Structures

PURIM LADPLI, CHEN LIU, FOTIS KOPSAFTOPOULOS
and FU-KUO CHANG

ABSTRACT

This work developed and evaluated an acousto-ultrasonic system that measures battery state of charge and, in particular, its state of health using a built-in, low-profile piezoelectric transducer system. A diagnostic method was proposed that relates changes in the guided wave signals to the charge, discharge, and aging processes, via electrochemically-induced changes in mechanical properties. A matching-pursuit-based feature extraction scheme was developed to allow an efficient, *in-operando* decomposition of signals into a set of predictors correlated with battery states. A particle filter framework was established which provides state estimation and remaining life prognostics to allow ultrasonic features to be used as measurements. It was shown on off-the-shelf Li-ion batteries and battery-integrated structures that the ultrasonic technique significantly improved the prediction performance and contained uncertainties.

INTRODUCTION

Extensive research effort in energy storage, particularly in lithium-ion (Li-ion) batteries, has been ongoing in response to the ever-growing demand for high-energy, light-weight energy solutions. Li-ion batteries are extremely complex systems with a very narrow operating range and are prone to premature and unexpected failure [1]. To optimize battery performance, lifespan, and most importantly, safety, a battery management system (BMS) is needed to perform battery condition monitoring and management [2]. To facilitate these functions, the BMS must first and foremost be able to accurately monitor the batteries' critical internal states. These primarily include state of charge (SoC) (the useful charge remaining in the battery with respect to its fully-charged capacity, or the equivalent of a fuel gauge) and state of health (SoH) (the degree

Purim Ladpli, Chen Liu, Fu-Kuo Chang, Department of Aeronautics and Astronautics, Stanford University, Stanford, CA, USA

Fotis Kopsaftopoulos, Department of Mechanical, Aerospace and Nuclear Engineering, Rensselaer Polytechnic Institute, Troy, NY, USA

of degradation in battery health which usually manifests as a reduction in the fully-charged capacity over time due to repeated usage) [2].

It is a true detriment to the field that the practical implementation of high-energy battery systems is still extremely challenging due to the lack of a field-deployable, yet affordable, BMS that can reliably and accurately monitor SoH [3]. While a range of measurement methods exist, most *in-operando* techniques are electrically-based and rely on measurement of the cell terminal voltage from a remote, centralized data acquisition unit. These methods are simple and work reasonably well for SoC estimation because of the highly-correlated SoC-voltage relationship, but they can be inaccurate and unreliable, particularly for SoH estimation [3].

The authors [4] and similar efforts in the field [5, 6] have recently introduced an ultrasound-based method for probing SoC and SoH of Li-ion batteries. These methods exploit the fact that mechano-electrochemical coupling is present when batteries undergo charging, discharging, and aging, which is detectable via ultrasound. In particular, we have shown that it is feasible to estimate battery SoC and SoH with ultrasonic guided waves using low-profile, built-in networks of piezoelectric actuators and sensors (Figure 1). This demonstrates that the technique can be made scalable and deployable in practical battery applications.

A continuation of our work is presented in this paper where special emphasis is given to the formulation of a systematic framework for estimating and providing prognosis of battery health. This paper explores how features extracted from ultrasonic signals may be used in a systematic framework to assess the internal state variables of a battery system as well as to perform prognostics of the remaining useful life (RUL). The ultrasonic features serve as indirect measurements where, together with the knowledge of a system's anticipated transition and historical data, inference and state estimation techniques may be applied to predict its state and remaining life.

The second contribution of this paper is the application and validation of the proposed prognostic framework on battery-integrated structures. The concept of multifunctional energy storage composites (MESC) was previously proposed by the authors [7]. MESC encapsulate lithium-ion battery materials inside high-strength carbon-fiber composites allowing batteries to contribute to mechanical load carrying capabilities. Here, the guided wave technique will be employed to estimate and provide prognosis of SoC and SoH as well as mechanically-induced electrical damage in MESC. The obtained results will be useful for validating the robustness of the framework in response to changing degradation mechanisms over the battery lifetime.
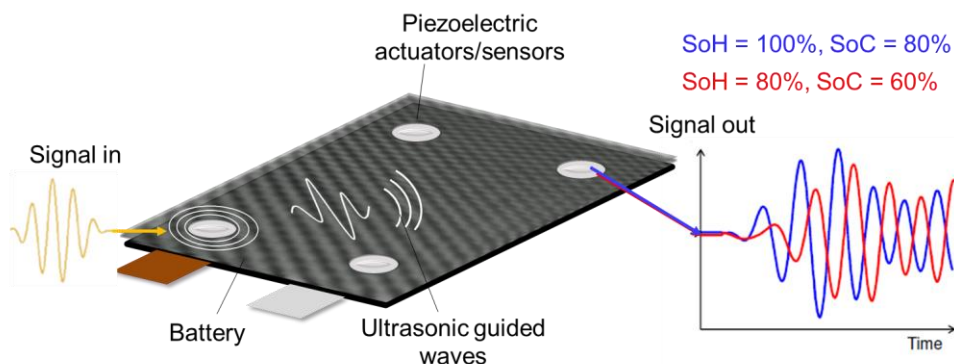

Figure 1. Schematics of ultrasonic guided-wave propagation in Li-ion battery substrate, using surface-mounted low-profile piezoelectric transducers.

PROBLEM STATEMENT

This study considers Li-ion batteries and battery-integrated structures with attached arrays of piezoelectric actuators and sensors (Figure 1). Given changes in sensor signals with respect to battery SoC and SoH, the goal of this study is to formulate an algorithm for extracting features from the ultrasonic signals and performing state estimation and prognostics of SoC and SoH. The specific objectives of this study are to:

1. Establish a systematic framework for encapsulating ultrasonic data into the state estimation and prognostics of battery SoC and SoH.
2. Generalize and validate the framework on MESC battery-integrated structures which involve mechanically-induced electrical degradation.

METHOD OF APPROACH

We first experimentally gather ultrasonic guided wave data at various SoC and SoH from the indicative Li-ion cells and MESC with surface-mounted piezoelectric transducer. A feature extraction scheme is proposed and established which allows in-operando ex-traction of a truncated set of predictive features that correlate with SoC and SoH. Finally, an SoC and SoH state estimation and prognostic model is developed which makes use of the extracted ultrasonic features and is validated for off-the-shelf Li-ion batteries as well as MESC.

EXPERIMENTS

Off-the-shelf Li-ion Pouch Batteries

Pitch-catch guided wave propagation experiments are performed on 3,650mAh off-the-shelf Li-ion pouch batteries (graphite/NCM chemistry) (AA Portable Power Corp.) (Figure 2 (A-B)). Guided wave signals are gathered at various battery SoC and SoH from surface-mounted, small-footprint piezoelectric disc transducers (6.35mm-diameter PZT-5A in the SMART Layer format; Acellent Technologies, Inc.) at the locations shown in Figure 2B. One of the piezoelectric discs can be chosen as an actuator to generate acousto-ultrasonic guided waves. The other piezoelectric disc then serves as a receiver to record the transmitted guided wave signals. The so-called "pitch-catch" experiments use five-peak Gaussian-windowed tone bursts with center frequencies between 100 to 200 kHz. The piezoelectric transducers are actuated and sensed using anultrasonic data acquisition system (ScanGenie II; Acellent Technologies, Inc.). Ultrasonic measurements are taken every 1 minute during electrical cycling.

The ultrasonic data acquisition is synchronized with the battery analyzer (BST8-3; MTI Corporation), which performs battery cycling. The cells are electrically discharged at an elevated temperature of 45°C with a constant current rate of 3,000 mA from 4.2V (100% SoC) to 3.0V (0% SoC). A total of 200 discharge cycles are performed. The remaining capacity for each cycle, which is our definition of SoH, was calculated by evaluating the cycle discharge capacity normalized with respect to the value from the first cycle. The cycle-to-cycle terminal voltage of a representative cell and its capacity fading (SoH degradation) characteristics are shown in Figure 2 (C-D).
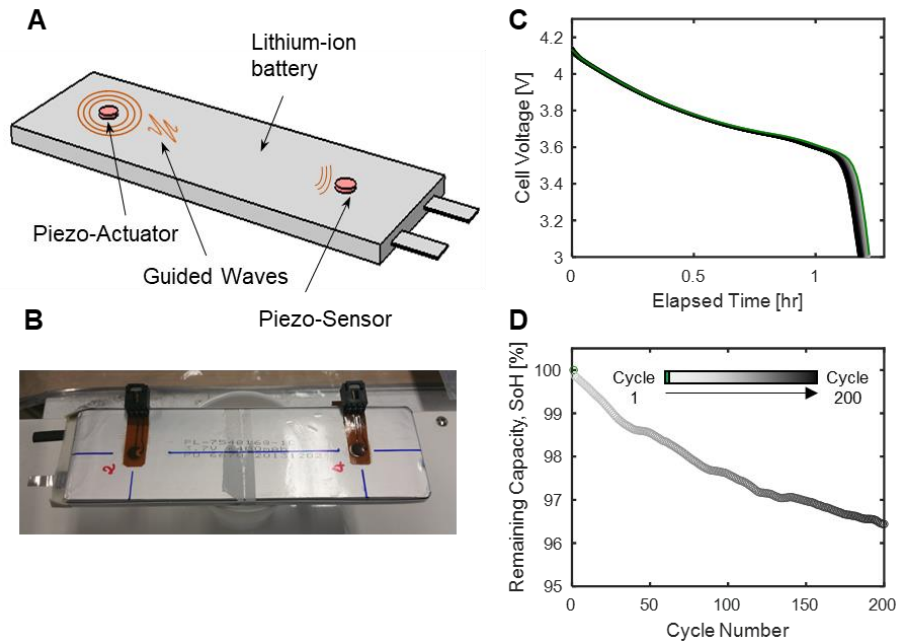
Figure 2. Experiment setup and results from 3,650 mAh batteries. (A) schematics of pitch-catch guided wave propagation. (B) experimental pouch cell with built-in piezos. (C) discharge curves during cycle life aging. (D) capacity retention plot.

MESC I-Beams with Mechanical Fatigue-induced SoH Aging

Structural battery I-beams consisting of 3 MESC cells are fabricated with the geometry shown in Figure 3 (readers are referred to [8] for further details regarding MESC I-beam architecture). The battery cells, each with a nominal capacity of 1.5 Ah, are integrated into the web of the I-beam and share a common electrolyte-encapsulating frame as shown. The web laminates (C-channels, T800/3900-2, $[\pm45]_s$ layup) simultaneously act as facesheets for batteries. The flanges ($[0_2]$ layup) are then attached to the I-beam via secondary bonding. Each battery in the I-beam is equipped with two piezoelectric transducers at the locations shown in Figure 3A. In addition to cycle life aging, The multi-cell MESC systemsalso undergo a mechanical fatigue test, which accelerates electrical degradation.

Figure 3 (C-D) show cycling data of Cell 1 in a representative MESC I-beam where the I-beams undergo 1C-rate cycle life aging at 50 °C for 100 cycles. At Discharge Cycle 50, the beam is subjected to mechanical fatigue by introducing a three-point-bending load for 1,000 cycles with a maximum load amplitude of 8,800 N (Figure 3B). Figure 3C shows the progression of the discharge curves due to electrical life cycle aging and mechanical fatigue. The discharge curves of the first 50 cycles before mechanical fatigue are shown in progressive shades of green, while those of the latter 50 cycles following the mechanical fatigue are shown in progressive shades of red. A noticeable shift is seen between Cycles 50 and 51 due to the mechanically-induced electrical damage from the mechanical fatigue as well as any inherent aging due to, for instance, storage during that period. This corresponds to the capacity fading behavior presented in Figure 3D, which also compares the capacity fading of the test cell to the nominal aging behavior of MESC cells that undergo the same accelerated cycle life aging, but not mechanical fatigue.
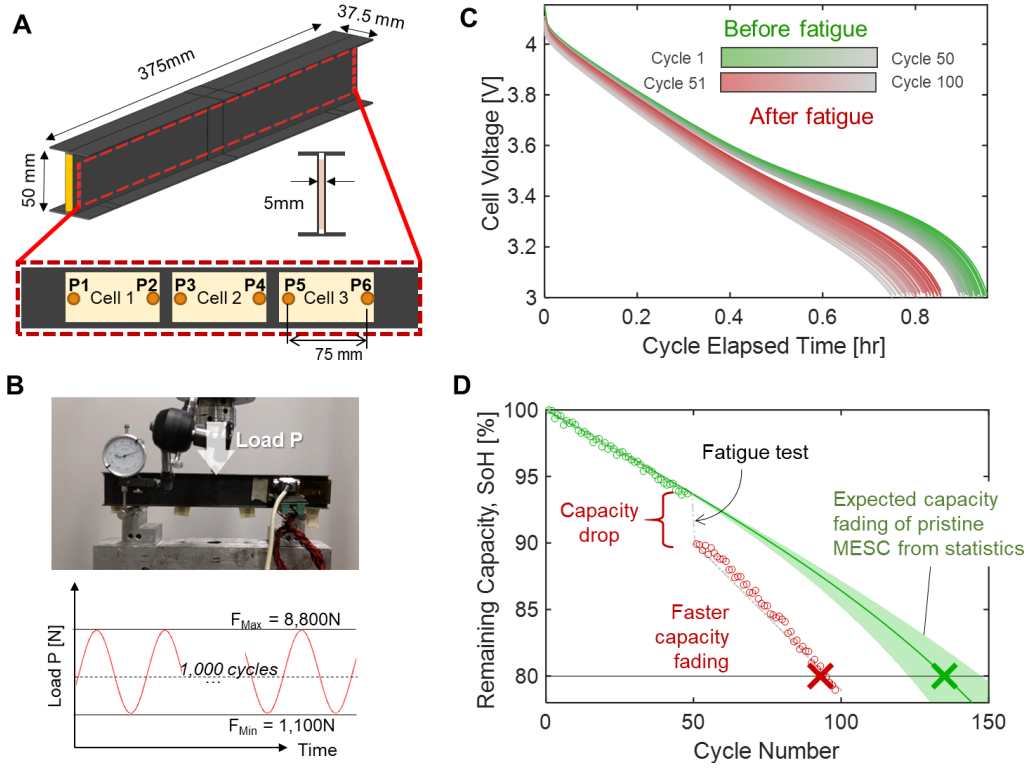
Figure 3. MESC I-beam with a surface-mounted network of piezoelectric transducers. (A-B) schematic of MESC I-beam and setup of fatigue experiment. (C-D) electrical data from cycle life aging – (green) pre-fatigue; (red) post-fatigue.

SIGNAL PROCESSING AND FEATURES EXTRACTION

An efficient strategy for signal processing and feature extraction based on the matching pursuit (MP) technique was presented in our previous work [9]. The proposed method decomposes complex waveforms into constituent 'atoms', allowing the time-frequency information of the signals to be mined. MP finds the best matching projections of the guided wave signals onto the span of a redundant dictionary of waveforms or atoms. We employ MP using the Gabor dictionary (a collection of scaled, translated, and modulated versions of Gaussian-windowed tone bursts) to decompose the guided wave responses into a linear expansion of constituent tone-burst atoms (Figure 4A).

At a given state, each atom m out of the total M extracted atoms can be represented by three parameters: (a_m, b_m, u_m); $m = [1, 2, …, M]$, which describe amplitude, phase, and speed of the tone burst. We then monitor the evolution of (a_m, b_m, u_m) with reference to changing SoC and SoH throughout the experiment. The Gabor parameters that encompass the entire range of SoC and SoH within the experiment are analyzed collectively. As an example, these results are shown in Figure 4B for a representative 3,650 mAh cell.
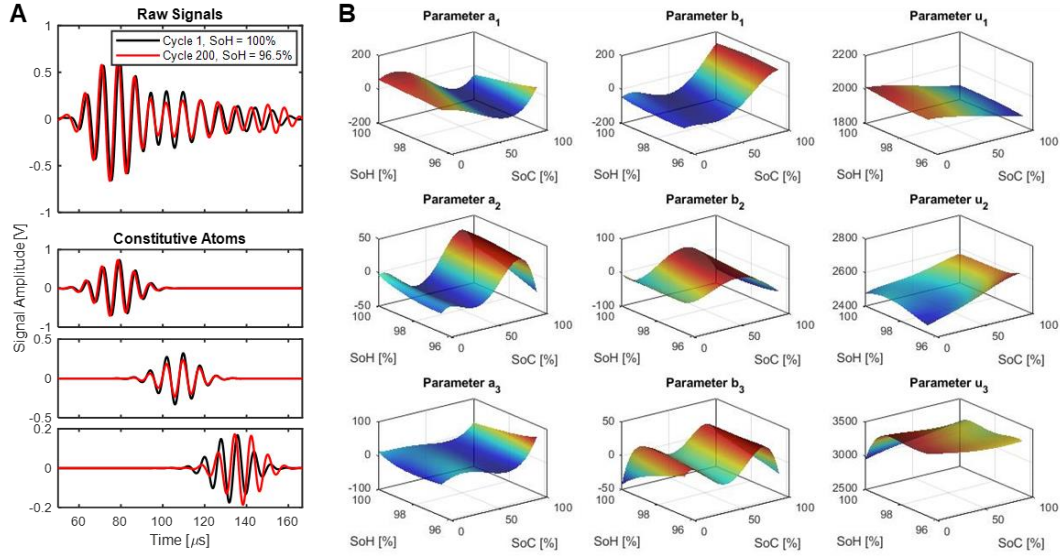
Figure 4. Feature extraction. (A) behavior of Gabor atoms due to the changes in SoH. (B) Gabor parameters (a_m, b_m, u_m) of the first three atoms as a function of SoC & SoH.

STATE ESTIMATION AND PROGNOSTICS

Model Identification

SoH degradation due to aging is associated with a decrease in the maximum available capacity, also referred to as capacity fading. Cycle life is an important parameter signifying the number of times a battery can be discharged before its maximum available capacity or SoH fades below an acceptable end-of-life (EoL) threshold. A sum of two exponential functions may be used to empirically model these non-linear capacity fading processes of many different batteries undergoing a variety of aging conditions [10, 11]. For a discrete-time process at time step k, this is written as:

$$SoH_k = \frac{Q_k}{Q_0} = C_{1,k}e^{-\lambda_1 k} + C_{2,k}e^{-\lambda_2 k} \tag{1}$$

where Q is the current battery capacity (Ah), Q_0 is the initial (pristine) battery capacity (Ah), C_1 and C_2 are parameters governing the initial capacity (%), λ_1 and λ_2 represent the aging rate (s^{-1}). Two nominally identical battery cells may not share the same set of parameters due to their inherent variabilities.

Once the SoH degradation model is established, the SoC can be expressed in differential form to take into account the instantaneous SoH. For a constant-current discharge process with a known input current, a discrete-time approximate recurrence can be written as:

$$SoC_k = SoC_{k-1} - \frac{i\Delta t}{SoH_k Q_0} \tag{2}$$

where i is the instantaneous electrical current (positive for discharge) (A) and Δt is the time increment at time step k (s).

SoH, SoC, C_1, λ_1, C_2, and λ_2 form the state vector of interest. Representative aging curves (SoH -vs- cumulative run time) of nominally identical batteries subjected to the

SOH

same usage are obtained. The relevant aging parameters C_1, λ_1, C_2, and λ_2 of each training cell are identified. The mean and variance of these parameters can then be calculated to indicate the expected behavior and the spread of the behavior of this type of battery undergoing this particular aging process.

The measurement update model was constructed from the functional relationships between the measurements (Gabor parameters of the constituent ultrasonic atoms (i.e. Figure 4B) as well as cell voltage) and SoC and SoH. Herein, statistical regression was used to generate representative response surfaces (measurement -vs- SoC and SoH). A 5th-order polynomial surface fit was chosen for its simplicity to model the response surfaces with respect to SoC and SoH. The measurement response surfaces can be expressed as follows:

$$\bar{\chi} = h_\chi(SoC, SoH) = \sum_{p=0}^{P} \sum_{q=0}^{P-p} A_{\chi\, p,q} (SoC)^p (SoH)^q \tag{3}$$

where $\bar{\chi}$ is the model predicted value of the measurements χ which include cell voltage, and the Gabor parameters; i.e. χ can be V, a_m, b_m, u_m ($m = 1, 2, \ldots, M$; where M = number of atoms extracted and utilized in prediction), P is the degree of the polynomial ($P = 5$, in this case), $A_{\chi\, p,q}$ are the corresponding polynomial coefficients.

State Estimation Formulation

Here, the concept is demonstrated using Bayesian techniques which are known to provide a general formal framework for dynamic state-estimation problems such as those with batteries [10, 11]. Special emphasis is on the particle filter (PF) approach which is regarded as an umbrella technique that can take into account non-linear systems with non-Gaussian noise. PF can estimate a probability density function (PDF) of the state using a recursive Bayesian filter with a Monte Carlo simulation. The construction of the PDF is based on all available measurement information which together contain the prediction uncertainty. Therefore, PF is chosen as an agnostic benchmark framework to compare typical cell voltage measurement to the performance of ultrasonic data. The state transition and measurement update of the PF framework can be constructed from the parametric models above (Equations (1), (2), and (3)). Then, we can write the dynamics of the system as a first-order Markov process:

State Transition:

$$\boldsymbol{X}_k \begin{cases} C_1: & x_{1,k} = x_{1,k-1} + \omega_{1,k} \\[1.5ex] \lambda_1: & x_{2,k} = x_{2,k-1} + \omega_{2.k} \\[1.5ex] C_2: & x_{3,k} = x_{3,k-1} + \omega_{3.k} \\[1.5ex] \lambda_2: & x_{4,k} = x_{4,k-1} + \omega_{4.k} \\[1.5ex] SoC: & x_{5,k} = x_{5,k-1} - \dfrac{i\Delta t}{x_{6,k} Q_0} + \omega_{5.k} \\[1.5ex] SoH: & x_{6,k} = x_{1,k} e^{-x_{2,k} k} + x_{3,k} e^{-x_{4,k} k} + \omega_{6.k} \end{cases} \tag{4}$$

Measurement Update:

$$Y_k \begin{cases} V: \quad y_{1,k} = \sum_{p=0}^{P} \sum_{q=0}^{P-p} A_{V\,p,q}\left(x_{5,k}\right)^p \left(x_{6,k}\right)^q + v_{1,k} \\[2mm] a_1: \quad y_{2,k} = \sum_{p=0}^{P} \sum_{q=0}^{P-p} A_{a_1\,p,q}\left(x_{5,k}\right)^p \left(x_{6,k}\right)^q + v_{2,k} \\[2mm] b_1: \quad y_{3,k} = \sum_{p=0}^{P} \sum_{q=0}^{P-p} A_{b_1\,p,q}\left(x_{5,k}\right)^p \left(x_{6,k}\right)^q + v_{3,k} \\[2mm] \quad\quad\quad\quad\vdots \\[2mm] u_M: \quad y_{3M+1,k} = \sum_{p=0}^{P} \sum_{q=0}^{P-p} A_{u_M\,p,q}\left(x_{5,k}\right)^p \left(x_{6,k}\right)^q + v_{3M+1,k} \end{cases} \quad (5)$$

where k is the time index, X denotes the state vector, Y is the output or measurement vector, and ω and v are the state and measurement noise as sampled from independent noise distributions. The initial values $x_{1,0}$, $x_{2,0}$, $x_{3,0}$, and $x_{4,0}$ are set to be the mean C_1, λ_1, C_2, and λ_2 values obtained from the least-squares fit of Equation (1) using the SoH degradation trends from a separate group of training cells. Therefore, $\omega_{1,0}$, $\omega_{2,0}$, $\omega_{3,0}$, and $\omega_{4,0}$ encapsulate the cell-to-cell variability that may be present, as well as the error inherent to the regression task. The SoC and SoH estimates at time step k are calculated from $x_{5,k}$ and $x_{6,k}$.

The PF algorithm approximates the PDF of the filtering distribution by a set of N weighted samples, or 'particles', $\{(w_k^i,\ X_k^i) : i = 1,\ 2, \dots, N\}$, where w_k^i is the importance weight of each particle X_k^i [12]. The crux of PF is to predict the probability density function (PDF) the particle distribution and the associated weights using:

$$p(X_k|Y_{0:k}) \approx \sum_{i=1}^{N} w_k^i\, \delta(X_k^i - \widehat{X}_k) \quad (6)$$

where $\delta(\cdot)$ is the Dirac delta function and the state mean $\widehat{X}_k$, or the state estimate, can be shown to be:

$$\widehat{X}_k = \sum_{i=1}^{N} w_k^i\, X_k^i \quad (7)$$

Here, the sampling importance resampling (SIR) is used which reduces the recursive weight updating to:

$$w_k^i = w_{k-1}^i\, p\left(Y_k \middle| X_k^i\right) \quad (8)$$

The weights w_k^i are then normalized to sum to 1. SIR also allows resampling to be performed when all but a small subset of particles have nearly zero importance weights. Resampling is done by drawing a new set of particles with $1/N$ weights from the discrete approximation of the posterior distribution when the effective number of particles $N_{eff} = \frac{1}{\sum_{i=1}^{N}(w_k^i)^2}$ falls below a certain threshold. The flowchart of the model identification and prediction process is shown in Figure 5.
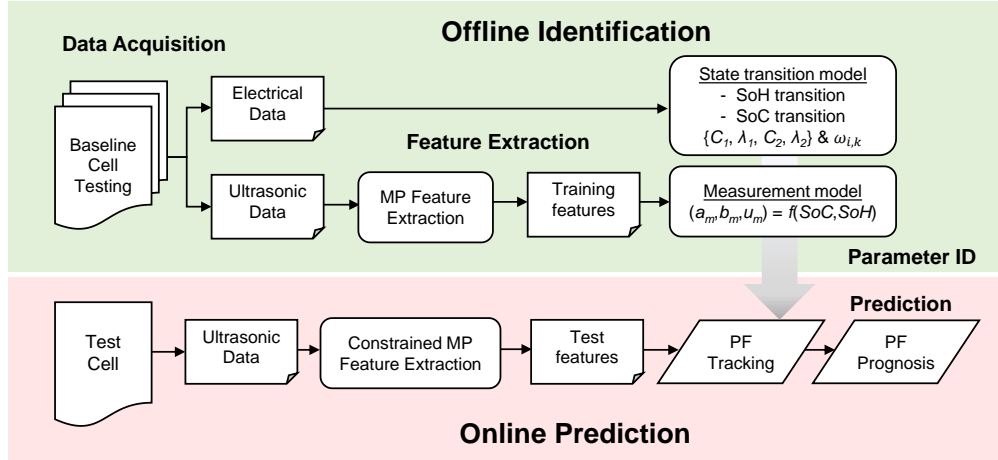

Figure 5. Flowchart of PF offline identification and online prediction.

STATE ESTIMATION AND PROGNOSTIC RESULTS

Off-the-shelf Li-ion Pouch Batteries

Figure 6 shows the SoH estimation and EoL prognostic results. Subfigures A, B, C, and D correspond to the models with $M = 0, 1, 2,$ and 3, respectively (increasing number of ultrasonic Gabor atoms). The green crosses represent the measured SoC, while the solid black line shows the PF tracking. Here, the PDFs represent the projection of particle distribution until SoH hit the predetermined EoL threshold. The prediction points are at Cycles 10, 50, and 90, which correspond to the red, green, and blue asterisks and PDFs respectively. The EoL threshold is set to SoH = 96.5% which corresponds to the actual EoL at Cycle 209 (red cross).

At every prediction point, the mean EoL predictions of the $M = 0$ model (cell voltage only) miss the actual EoL by approximately 100 cycles. The addition of ultrasonic features is shown to dramatically improve the PF performance by landing the PDFs more precisely on the actual EoL and with a higher confidence level. With $M = 3$, the mean EoL predictions miss the actual value by only 3-6 cycles at any prediction point. he standard deviation of the estimated EoL is also reduced to only 2-3 cycles as opposed to ~35 cycles when only cell voltage is used. This demonstrates the effectiveness of ultrasonic data, which are more strongly correlated with SoH than cell voltage measurements, in improving the SoH estimation and EoL prognostics.
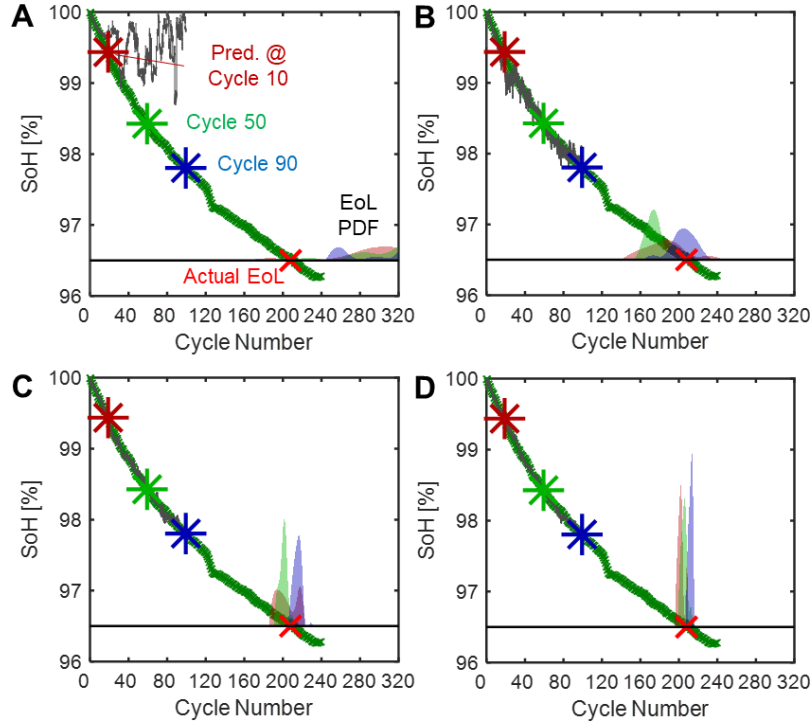
Figure 6. EoL (SoH) prognostic results on the test 3,650 mAh cell. (A), (B), (C), and (D) comparison of EOL PDFs obtained from PF models with $M = 0$, 1, 2, and 3, respectively.

MESC I-Beams with Mechanical Fatigue-induced SoH Aging

The prognostic results on the test MESC cell are shown in Figure 7. Subfigures A, B, and C correspond to the models with $M = 0$, 1, and W3, respectively. There are prediction points both before and after mechanical fatigue. The pre-fatigue prediction points are at Cycles 20 and 40 which correspond to green and dark green asterisks and EoL PDFs, whereas post-fatigue predictions are made at Cycles 60 and 80 which are represented by red and dark red asterisks and PDFs. The EoL threshold is set to 80%, which corresponds to an actual EoL at Cycle 93 for the damaged cell (red cross) and at Cycle 135 for nominal MESC cells that do not undergo mechanical fatigue (green cross).

The PF which uses cell voltage cannot discern the effect of mechanical fatigue resulting in an EoL prediction that does not adapt to the varying aging rates and capacity drops. On the other hand, the addition of ultrasonic features allows PF to more accurately track the SoH progression as well as allow the aging parameters to be updated correctly according to the pre- and post-fatigue stages. This can be seen from a change of course of PF tracking immediately following the mechanical fatigue which tracks the new fading curve precisely after several cycles. The pre- and post-fatigue EoL PDFs are also clearly segregated as a result of the coefficients in the aging equation being updated.
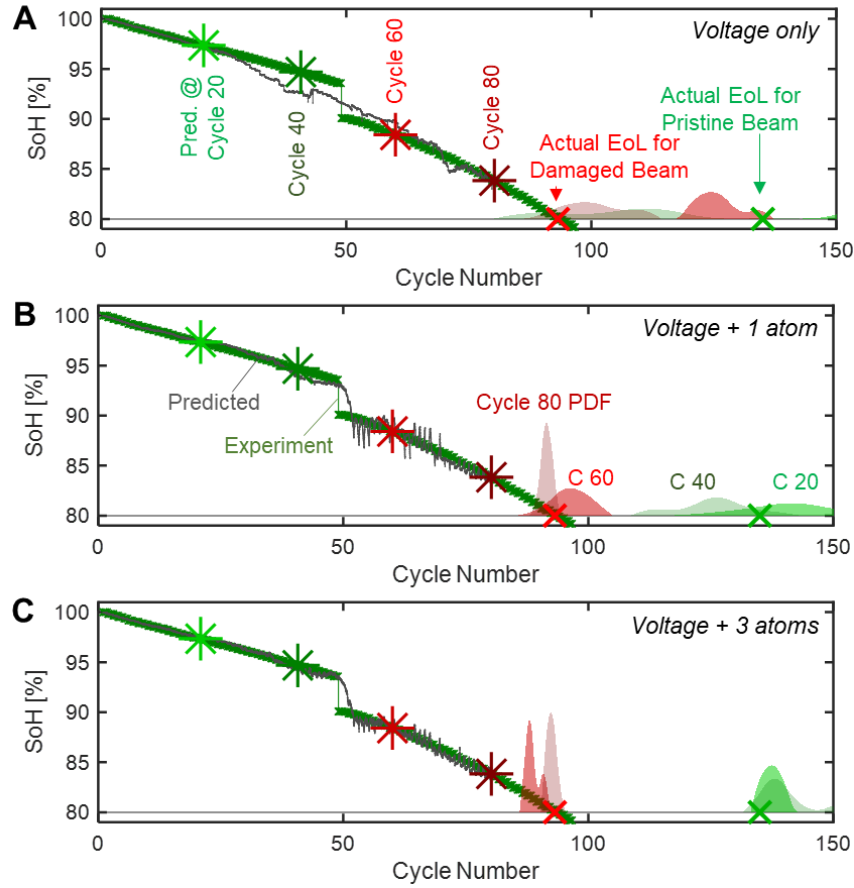
Figure 7. EoL (SoH) prognostic results on test MESC I-beam showing adaptability of PF to fatigue-induced electrical damage. (A) PF model which uses only cell voltage as predictor showing poor segregation of EoL PDFs between pre-fatigue (green PDFs) and post-fatigue (red PDFs). (B) and (C) PF models which, in addition to cell voltage, include Gabor parameters from 1 and 3 atoms, respectively.

CONCLUSION REMARKS

An acousto-ultrasonic system was developed which uses built-in, low-profile piezoelec-tric sensors to propagate guided waves for monitoring of battery SoC and SoH. While traditional cell voltage measurements are not sensitive to SoH, guided wave signals were found to strongly correlate with the changes in electrodes mechanical properties during both cycling and aging. This allows in-operando estimation and remaining useful life prognostics to be performed for SoC and, particularly, SoH with significantly better accuracy than using voltage measurements.

An MP-based feature extraction algorithm was proposed as an efficient means to perform signal analysis and condense high-dimensional guided wave data into a reduced set of important predictive features. A waveform is decomposed into constituent Gabor atoms whose descriptive parameters form functional relationships with respect to SoC and SoH. A PF framework was formulated to provide real-time estimation and RUL prognostics of SoC and SoH. This framework utilizes the extracted ultrasonic features as additional measurements in order to better contain the prediction uncertainty. Finally, the concept was demonstrated on MESC I-beams which the ultrasonic system was also effective in tracking and adapting to electrical damage induced by mechanical loading.

ACKNOWLEDGEMENTS

REFERENCES

1. Etacheri, V., R. Marom, R. Elazari, G. Salitra, and D. Aurbach, *Challenges in the development of advanced Li-ion batteries: a review.* Energy & Environmental Science, 2011. **4**(9): p. 3243-3262.
2. Waag, W., C. Fleischer, and D.U. Sauer, *Critical review of the methods for monitoring of lithium-ion batteries in electric and hybrid vehicles.* Journal of Power Sources, 2014. **258**: p. 321-339.
3. Zhang, J. and J. Lee, *A review on prognostics and health monitoring of Li-ion battery.* Journal of Power Sources, 2011. **196**(15): p. 6007-6014.
4. Ladpli, P., F. Kopsaftopoulos, and F.-K. Chang, *Estimating state of charge and health of lithium-ion batteries with guided waves using built-in piezoelectric sensors/actuators.* Journal of Power Sources, 2018. **384**: p. 342-354.
5. Gold, L., T. Bach, W. Virsik, A. Schmitt, J. Müller, T.E. Staab, and G. Sextl, *Probing lithium-ion batteries' state-of-charge using ultrasonic transmission–Concept and laboratory testing.* Journal of Power Sources, 2017. **343**: p. 536-544.
6. Hsieh, A., S. Bhadra, B. Hertzberg, P. Gjeltema, A. Goy, J. Fleischer, and D. Steingart, *Electrochemical-acoustic time of flight: in operando correlation of physical dynamics with battery charge and health.* Energy & environmental science, 2015. **8**(5): p. 1569-1577.
7. Ladpli, P., R. Nardari, F. Kopsaftopoulos, and F.-K. Chang, *Multifunctional energy storage composite structures with embedded lithium-ion batteries.* Journal of Power Sources, 2019. **414**: p. 517-529.
8. Ladpli, P., R. Nardari, Y. Wang, P.A. Hernandez-Gallegos, R. Rewari, H.T. Kuo, F. Kopsaftopoulos, K.D. Kepler, H.A. Lopez, and F. Chang, *Multifunctional Energy Storage Composites for SHM Distributed Sensor Networks*, in *International Workshop on Structural Health Monitoring 2015*. 2015: Stanford, CA.
9. Ladpli, P., C. Liu, F. Kopsaftopoulos, and F.-K. Chang. *Estimating Lithium-ion Battery State of Charge and Health with Ultrasonic Guided Waves Using an Efficient Matching Pursuit Technique*. in *2018 IEEE Transportation Electrification Conference and Expo, Asia-Pacific (ITEC Asia-Pacific)*. 2018. IEEE.
10. He, W., N. Williard, M. Osterman, and M. Pecht, *Prognostics of lithium-ion batteries based on Dempster–Shafer theory and the Bayesian Monte Carlo method.* Journal of Power Sources, 2011. **196**(23): p. 10314-10321.
11. Saha, B., K. Goebel, S. Poll, and J. Christophersen, *Prognostics methods for battery health monitoring using a Bayesian framework.* IEEE Transactions on instrumentation and measurement, 2009. **58**(2): p. 291-296.
12. Arulampalam, M.S., S. Maskell, N. Gordon, and T. Clapp, *A tutorial on particle filters for online nonlinear/non-Gaussian Bayesian tracking.* IEEE Transactions on signal processing, 2002. **50**(2): p. 174-188.